ASPECT RATIO EFFECT ON LAMINAR FLOW BIFURCATIONS IN A CURVED RECTANGULAR TUBE DRIVEN BY PRESSURE GRADIENTS

K. T. Chen

Department of Applied Mathematics
National Chung Hsing University
Taichung, Taiwan

K. F. Yarn

Department of Electronic Engineering
Far East University
Tainan, Taiwan

H. Y. Chen **C. C. Tsai**

Department of Applied Mathematics
National Chung Hsing University
Taichung, Taiwan

W. J. Luo*

Graduate Institute of Precision Manufacturing
National Chin-Yi University of Technology
Taichung, Taiwan

C. N. Chen

Department of Physics
Tamkang University
New Taipei, Taiwan

ABSTRACT

This study investigated the flow bifurcations of flows driven by a pressure gradient in a rectangular curved tube. When fluid flows within a curved tube, due to the centrifugal effect, secondary vortices can be induced in the cross section of the tube. The secondary flow states are dependent on the magnitude of the pressure gradient (q) and the aspect ratio (γ). In this study, the continuation method was applied to investigate the flow bifurcations in a curved tube with increasing pressure gradient ($1 < q < 6000$) and aspect ratio ($0.9 < \gamma < 1.4$).

The bifurcation diagrams are composed of solution branches, which are linked by limiting points or bifurcation points. The flow states in a solution branch belong to the same group. The ranges of the flow states and the relationship between the states can also be derived from the bifurcation diagrams. In this study, two types of bifurcation were found, one in the range of $0.9 < \gamma < 1.17$, and another in the range of $1.18 < \gamma < 1.4$. The ranges of stable flow solutions and the distributions of limit and bifurcation points in both pressure gradient and aspect ratio are derived in this study.

Keywords: Pressure gradient, Rectangular curved tube, Flow bifurcation, Aspect ratio effect.

* Corresponding author (wjluo@ncut.edu.tw)

DOI : 10.1017/jmech.2017.93
Copyright © 2017 The Society of Theoretical and Applied Mechanics
https://doi.org/10.1017/jmech.2017.93 Published online by Cambridge University Press

1. INTRODUCTION

The fluid state inside a curved tube involves many important phenomena in fluid dynamics, such as fluid stability, flow bifurcation, the existence of multiple solutions and flow field states. In the design and application of industrial or biomedical components, such as industrial pipeline designs, or human blood and respiratory flows, fluid conditions inside curved tubes must be considered. When a fluid flows through a curved tube, centrifugal force results in a vortex motion of the fluid on the cross section of the curved tube. If this secondary flow is represented as streamline on the cross section of the curved tube, there will be two mutually symmetrical vortices rotating in opposite directions; this is called a 2-cell flow field. As flow field states inside curved tubes drew more research attention, 4-cell flow fields were predicted, and 4-cell flow fields were found in circular and semicircular curved tubes by numerical simulations. After this, flow fields in curved tubes with rectangular sections were discussed in experimental validation, and the changes in curved tube curvature and pressure gradient were further studied.

The research and development of steady-state flow fields in curved tubes have evolved over a long history. Dean [1] proposed the dimensionless parameter, i.e. the Dean Number, combined with Reynolds number and curvature radius in 1928, so as to characterize the fully developed curved tube flow field. In the early stages, there were only two mutually contra rotational vortex flow fields found in the curved tube. More recently, a 4-cell flow field was found with an additional pair of small symmetrical vortices near the outer wall of the curved tube [2, 3]. In experimental validation, Hille *et al*. [4] discussed the 4-cell flow field in rectangular curved tube. Winters [5] applied the continuation method to discuss the probable patterns of flow field in different curvature radii, aspect ratios and different pressure gradients. The flow field patterns found in various curvature radii and pressure gradients were used to build a flow field bifurcation diagram. The mechanism of cross-correlation between various flow field patterns was discussed according to the bifurcation diagram.

Recently, Gauthier *et al*. [6] experimentally investigated the centrifugal instabilities of a flow in a curved rectangular tube with small aspect ratio. A threshold value Dean number was found, above which streamwise vortices were observed. Yanase *et al*. [7] used the spectral method to predict the flow patterns in a curved rectangular duct over a wide range of aspect ratio. In their study, five steady state flow solutions were found, among which one steady solution was stable for most aspect ratios, and the other two steady solutions were stable for small aspect ratios. However, the evolutions of the corresponding bifurcation diagrams and the existence regions in terms of the pressure gradient and aspect ratio were not investigated in detail.

Yamamoto *et al*. [8] used the spectral method to investigate the flow in a curved rectangular tube whose walls, except for the outer wall, rotated around the curvature center of the tube. In their study, four-vortex, eight-vortex and asymmetric flow states were found in the curved tube, depending on the rotation speeds of the tube and azimuthal driving pressure gradients. Yamamoto *et al*. [9] also conducted experiments to visualize the induced secondary flows in a curved tube whose walls, except for the outer wall, rotated around the curvature center of the tube. The observed flow patterns in the curved tube were in agreement with the numerical results. Bhunla and Chen [10] numerically investigated the laminar flow characteristics in a curved rectangular tube with variable cross section. Norouzi *et al*. [11] and Norouzi and Biglari [12] numerically simulated the inertial and creeping flow of a viscoelastic fluid in a curved square tube, and showed that the flow within the tube can be stabilized by a negative second normal stress difference of the fluid, but be destabilized by a first normal stress difference of the fluid.

Researching time-dependent flow fields inside curved rectangular tubes, Wang and Yang [13] found evidence of periodic oscillation between symmetric/asymmetric 2-vortex flow states and symmetric/asymmetric 4-vortex flow states. A periodic flow solution was found in a curved square tube by Mondal *et al*. [14], who adopted the spectral method to construct a flow bifurcation diagram, while the Dean number exceeded the values of the pitchfork or Hopf bifurcation point. Komai and Tanishita [15] used the numerical method to discuss the time-dependent and fully developed flow field inside an extremely curved tube, so as to simulate cardiovascular flow. They found that the flow field state of a secondary flow inside the curved tube was influenced by diastolic period. Hüttl and Friedrich [16] applied the second-order accurate finite volume method for numerical simulation of the turbulence in curved and helically coiled tubes in orthogonal helical coordinates. They found that the tube curvature significantly influenced the secondary flow rate, and the torsional effect of helical tube was weaker than the curvature effect. Cioncolini and Santini [17] studied the flow situation when a laminar flow transited to turbulent flow inside a helical tube. Ko and Ting [18] analyzed a fully developed steady laminar flow inside a helical tube, discussed the variance in curvature and Reynolds number, and used the least square error to analyze the numerical results.

Examining non-isothermal flow through a curved rectangular tube, Liu and Wang [19], Mondal *et al*. [20] and Mondal and Islam [21] numerically studied non-isothermal flows with convective heat transfer in a curved square tube with a temperature difference between the hot outer wall and cool inner wall, using the spectral method. It was found that, with an increase in the Dean number, the steady state flow becomes a periodic flow, and then transforms to a chaotic flow in the curvature range of 0.001 to 0.5, and that the heat transfer increases significantly with the temperature difference between the walls.

According to a recent discussion of steady-state flow fields inside circular or semicircular curved tubes, when the Dean number exceeds specific threshold values, multiple flow field states occur inside the curved tube, specifically 2-cell and 4-cell flow states. When the Dean

https://doi.org/10.1017/jmech.2017.93 Published online by Cambridge University Press

number for a flow field inside a rectangular curved tube is greater than a specific threshold, a 4-cell flow field occurs by transition from the original 2-cell flow field.

Although steady-state flow fields inside rectangular curved tubes has been extensively studied, the evolution of bifurcation diagrams and the existing range of stable flow states in terms of pressure gradient and aspect ratio in steady-state flow fields inside rectangular curved tubes are rarely determined.

Therefore, this study focused on flow field states inside curved rectangular tubes, induced flow field states, bifurcation evolutions and threshold values of driving pressure gradients with the variation of aspect ratio. This was achieved by examining a curved tube with a rectangular section, while manifold steady state flow solutions were determined by continuation method [22], through which flow solution branches and bifurcation diagrams can be constructed in terms of pressure gradient and aspect ratio. Then, a linear stability analysis was used to determine whether the flow solutions in each solution branch were stable or unstable. The primary purpose of this study is to provide detailed illustration of the complete bifurcation diagram evolution, and to determine the manifold solution branches and flow solutions in the bifurcation diagrams in terms of pressure gradient and aspect ratio. The second aim of this study is to distinguish existing ranges of stable flow solutions in terms of aspect ratio and pressure gradient.

2. MATHEMATICAL MODEL AND NUMERICAL METHODS

2.1 Governing Equations

This paper assumes that a flow field in a rectangular curved tube is an incompressible Newtonian flow, as shown in Fig. 1. Half of the width in *X*-direction of the rectangular section is *A*, half of the height in *Y*-direction is *B*, the curvature radius of the curved tube is *C*, the bending angle is Φ and the curved tube is full of Newtonian fluid with viscosity and density as constants. No-slip is used as a boundary condition and the pressure gradient is adopted as the variable continuation parameter for numerical simulations by continuation method.

In a curved rectangular tube, a laminar, steady, fully developed flow within a curved tube is considered. The flow field in the curved tube is assumed to be axial symmetric around the *T* axis. As shown in Fig. 1, in order to convert the left coordinate system (*R, T,* Φ) into the right coordinate system (*X, Y, Z*), the velocities on various axes of the cylindrical coordinate system are replaced by $u = u_R$, $v = u_Y$, and $w = u_\Phi$. The conversion equations for the two coordinate systems are $X = R\text{-}C$ and $dZ = Rd\Phi$. The following dimensionless parameters are used for problem analysis:

$$\bar{x} = \frac{x}{A}, \quad \bar{y} = \frac{Y}{B}, \quad \bar{z} = \frac{Z}{A}, \quad \bar{u} = \frac{u}{(\sigma / A)}, \quad \bar{v} = \frac{v}{(\sigma / A)},$$

$$\bar{w} = \frac{w}{(\sigma / A)}, \quad \bar{p} = \frac{p}{(\rho\sigma^2 / A^2)}, \quad \bar{t} = \frac{t}{(A^2 / \sigma)},$$

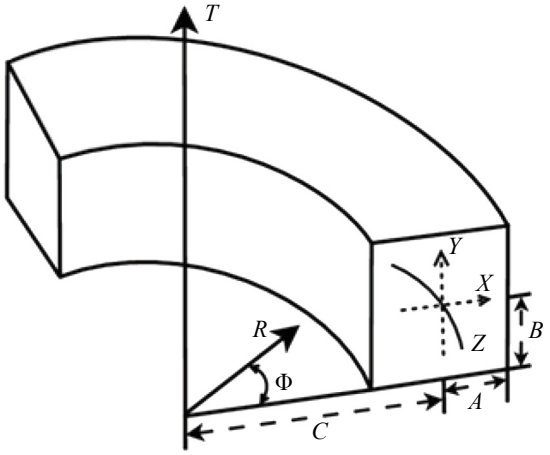


Fig. 1. Rectangular curved tube model.

where σ and ρ represent the kinematic viscosity and density of the fluid in the tube. The following dimensionless governing equation can be obtained from reduced and dimensionless derivation. In order to reduce the equation, the horizontal line marks on various dimensionless parameters shown above are omitted.

Continuation equation:

$$\frac{1}{(x+\beta)}\frac{\partial}{\partial x}[(x+\beta)u] + \frac{1}{\gamma}\frac{\partial v}{\partial y} = 0, \tag{1}$$

where the aspect ratio $\gamma = B/A$ and β is the non-dimensional radius of curvature, which is defined as $\beta = C/A$. The Navier-Stokes equations (Momentum conservation equations in (*x, y, z*)) are as follows:

x direction:

$$\frac{\partial u}{\partial t} + u\frac{\partial u}{\partial x} + \frac{v}{\gamma}\frac{\partial u}{\partial y} - \frac{w^2}{(x+\beta)} + \frac{\partial p}{\partial x}$$

$$-\nabla^2 u + \frac{u}{(x+\beta)^2} = 0, \tag{2}$$

y direction:

$$\frac{\partial v}{\partial t} + u\frac{\partial v}{\partial x} + \frac{v}{\gamma}\frac{\partial v}{\partial y} + \frac{1}{\gamma}\frac{\partial p}{\partial y} - \nabla^2 v = 0, \tag{3}$$

z direction:

$$\frac{\partial w}{\partial t} + u\frac{\partial w}{\partial x} + \frac{v}{\gamma}\frac{\partial w}{\partial y} + \frac{uw}{(x+\beta)} + \frac{\beta}{(x+\beta)}q$$

$$-\nabla^2 w + \frac{w}{(x+\beta)^2} = 0, \tag{4}$$

where (*u, v, w*) are the velocity vectors in (*x, y, z*) directions, *w* is axial velocity in *z* direction, and *q* is the pressure gradient in *z*-direction, i.e. $\frac{\partial p}{\partial z}$, and

$$\nabla^2 = \frac{1}{(x+\beta)}\frac{\partial}{\partial x}(x+\beta)\frac{\partial}{\partial x} + \frac{1}{\gamma^2}\frac{\partial^2}{\partial y^2}.$$

https://doi.org/10.1017/jmech.2017.93 Published online by Cambridge University Press

In order to express the aforesaid governing equation as a stream function-vorticity formulation, the stream function S is defined as:

$$u=\frac{\beta}{(x+\beta)\gamma}\frac{\partial S}{\partial y},\quad v=-\frac{\beta}{x+\beta}\frac{\partial S}{\partial x}, \tag{5}$$

and S is given by

$$\frac{(x+\beta)}{\beta}\left(\frac{\partial v}{\partial x}-\frac{1}{\gamma}\frac{\partial u}{\partial y}\right)-\frac{2}{(x+\beta)}\frac{\partial S}{\partial x}+\nabla^2 S=0.$$

The detailed derivation of the above equations can refer to Winters [5]. The vorticity function Ω is defined as:

$$\Omega=\frac{x+\beta}{\beta}\left(\frac{\partial v}{\partial x}-\frac{1}{\gamma}\frac{\partial u}{\partial y}\right). \tag{6}$$

Equation (5) is substituted into Eq. (6) to obtain the stream and vorticity function equation:

$$\Omega+\frac{\partial^2 S}{\partial x^2}+\frac{1}{\gamma^2}\frac{\partial^2 S}{\partial y^2}-\frac{1}{x+\beta}\frac{\partial S}{\partial x}=0. \tag{7}$$

In order to reduce the part related to pressure p in Eqs. (2) and (3), a curl operator was applied to Eqs. (2) and (3), i.e. ∂(eq. 2))/∂y − ∂(eq. (3)/∂x) [23, 24]. Due to steady state assumption, the unsteady state terms in Eqs. (2) and (3) are disregarded, and the vorticity transport equation can be obtained as:

$$\beta\frac{\partial S}{\partial y}\frac{\partial \Omega}{\partial x}-\frac{2\beta}{(x+\beta)}\frac{\partial S}{\partial y}\Omega-\beta\frac{\partial S}{\partial x}\frac{\partial \Omega}{\partial y}-\gamma(x+\beta)\frac{\partial^2 \Omega}{\partial x^2}$$
$$+\gamma\frac{\partial \Omega}{\partial x}-\frac{(x+\beta)}{\gamma}\frac{\partial^2 \Omega}{\partial y^2}+2w\frac{(x+\beta)}{\beta}\frac{\partial w}{\partial y}=0. \tag{8}$$

Equation (5) is substituted into Eq. (4), and the Navier-Stokes equation in z-direction is obtained as:

$$\beta\frac{\partial S}{\partial y}\frac{\partial w}{\partial x}-\beta\frac{\partial S}{\partial x}\frac{\partial w}{\partial y}+\beta\frac{w}{x+\beta}\frac{\partial S}{\partial y}+\gamma(x+\beta)q-\gamma\frac{\partial w}{\partial x}$$
$$-\gamma(x+\beta)\frac{\partial^2 w}{\partial x^2}-\frac{(x+\beta)}{\gamma}\frac{\partial^2 w}{\partial y^2}+\frac{\gamma w}{(x+\beta)}=0 \tag{9}$$

As the velocity of fluid on various tube walls meets the no-slip boundary condition, namely, zero velocity, according to the definition of Eq. (5), $\partial S/\partial x = \partial S/\partial y = 0$. Thus, at the top and bottom walls, the vorticity function equation can be written as $\Omega + (1/\gamma)\partial^2 S/\partial y^2 = 0$ and at the right and left walls, the vorticity function equation can be written as $\Omega + \partial^2 S/\partial x^2 = 0$, respectively. As the fluid will not penetrate through the boundary, the stream function value on various boundaries is constant. The stream function value on various boundaries can be defined as zero. By solving the stream and vorticity function Eq. (7), vorticity transport Eq. (8) and Navier-Stokes equation in z-direction Eq. (9), the manifold fully developed flow solutions in the curved rectangular tube in terms of different pressure gradients can be calculated by continuation method.

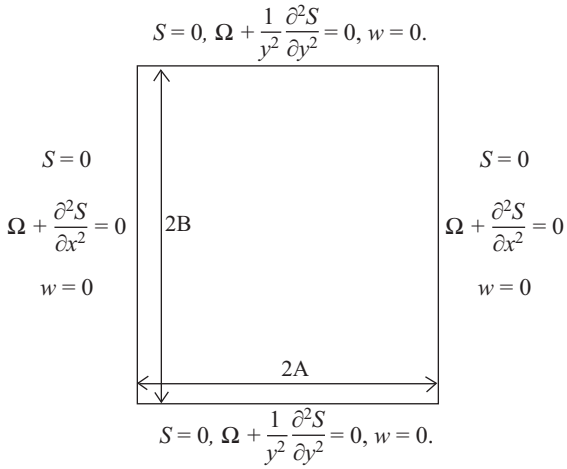


Fig. 2. Boundary conditions of a section of rectangular curved tube.

As shown in Fig. 2, the boundary conditions can be expressed as follows:

1. Top tube wall of rectangular curved tube section:

$$S=0,\quad \Omega+\frac{1}{\gamma^2}\frac{\partial^2 S}{\partial y^2}=0,\quad w=0.$$

2. Bottom tube wall of rectangular curved tube section:

$$S=0,\quad \Omega+\frac{1}{\gamma^2}\frac{\partial^2 S}{\partial y^2}=0,\quad w=0.$$

3. Left tube wall of rectangular curved tube section:

$$S=0,\quad \Omega+\frac{\partial^2 S}{\partial x^2}=0,\quad w=0.$$

4. Right tube wall of rectangular curved tube section:

$$S=0,\quad \Omega+\frac{\partial^2 S}{\partial x^2}=0,\quad w=0.$$

2.2 Numerical Method

In this study, the manifold steady state flow solutions were determined by continuation method through which flow solution branches and bifurcation diagrams can be constructed in terms of pressure gradient and aspect ratio. In the continuation method, first, central finite difference with second–order accuracy is applied to discretize differential governing Eqs. (7) ~ (9), and a matrix G composed of non-linear algebraic equations can be obtained:

$$G(V,q)=0, \tag{10}$$

where V is a solution vector and q is the parameter of pressure gradient in azimuthal direction of the governing equations. By taking a derivation of matrix G with respect to the solution vector V, (Dg/dV), an iterative sequence $V^{(k)}(q)$ can be obtained from matrix G, which can be expressed as:

https://doi.org/10.1017/jmech.2017.93 Published online by Cambridge University Press

$$V^{(0)}(q) \equiv \text{initial estimate}, \tag{11a}$$

$$G_V(q^{(k)}(q))[V^{(k+1)} - V^{(k)}] = -G(V^{(k)}, q), \quad k = 0,1,2, \tag{11b}$$

where G_V is the Jacobian matrix of matrix G. Through the iterative sequence, the solution vector $V(q)$ corresponding to a specific pressure gradient can be obtained when the iterative sequence reaches convergence.

In order to obtain a suitable initial estimate, $V^{(0)}(q)$, in the above iterative calculation, a Taylor expansion is applied to the solution vector, $V(q)$, with respect to tiny increment in parameter q.

$$V(q + \delta q) = V(q) + \delta q V_q(q). \tag{12a}$$

In Eq. (12a), the solution vector of $V_q(q)$ can be obtained from Eq. (12b) which is derived from Eq. (10) with respect to $V(q)$.

$$G_V(V, q) = -G_q(V, q)V_q \tag{12b}$$

The iterative calculation methodology in Eqs. (11) and (12) refers to the Euler-Newton continuation method, which is very effective for solution vector calculation with quadratic convergence. However, the iterative methodology cannot work at the singular points where the determinant value of the Jacobian matrix G_q approaches zero. In order to avoid this difficulty, an additional constraint equation, Eq. (13), is introduced into the iterative sequence:

$$\begin{aligned} &N(V(s), q(s)) \equiv \dot{V}(s_0) \cdot [V(s) - V(s_0)] \\ &+\dot{q}(s_0)[q(s) - q(s_0)] - (s - s_0) = 0, \end{aligned} \tag{13}$$

where parameter s is an arclength of the continuation calculation, and $[V(s_0), q(s_0)]$ are a previous convergent solution for a specific value of q. Moreover, $[\dot{V}, \dot{q}]$ denote $[dV/ds, dq/ds]$ which are tangent vectors of the solution vector $[V(s), q(s)]$ in terms of arclength length.

By integrating Eq. (10) and constraint Eq. (13), an augmented matrix can be obtained:

$$\begin{Bmatrix} G(V, q) = 0 \\ N(V, q, s) = 0 \end{Bmatrix}$$

The Jacobian matrix of the augmented matrix with respect to (V, q) can be expressed as:

$$\frac{\partial(G, N)}{\partial(V, q)} = \begin{pmatrix} G_V & G_q \\ N_V & N_q \end{pmatrix} \tag{14}$$

Using the iterative calculation methodology employed in Eqs. (11) and (12), the solution vector around the singular points can be determined [23-26].

2.3 Linear Stability Analysis Method

In order to determine the stability of the manifold flow solutions obtained by the above continuation method, a linear stability analysis was adopted. First, a small time perturbation was added to the flow solution, $V(q)$, calculated by the continuation method, expressed as:

$$V(q, t) = V(q) + \varepsilon e^{\delta t}, \tag{15}$$

where ε is a small perturbation vector.

In order to investigate the time dependent response of the flow solution to the small time perturbation, a time-dependent matrix derived from unsteady governing equations can be written as:

$$M(V)\frac{dV(q,t)}{dt} = G(V, q), \tag{16}$$

where $M(V)$ is the mass matrix. Substitute the time dependence flow solution, $V(q,t)$, in Eq. (15) into Eq. (16) and rearrange the terms of perturbation vector ε, and Eq. (16) can be rewritten as a generalized eigenvalue matrix form:

$$\delta M(V(q))\varepsilon = \tilde{J}(V(q))\varepsilon, \tag{17}$$

where $\tilde{J}$ denotes the Jacobian matrix of $G(V(q),q)$.

By solving the above eigenvalue matrix [27], the engenvalue matrices and their corresponding engenvectors, i.e. the small time perturbation vectors, can be obtained. The stability of the flow solutions can determine by the signs of their calculated eigenvalues, δ. If the real parts of all calculated eigenvalues are less than 0, then the small time perturbations will gradually decay over time. Thus, the corresponding flow solution, $V(q)$, can be recognized as a stable flow state. However, if the real part of at least one engenvalue among the calculated eigenvalues is greater than 0, then the corresponding time dependent perturbation will gradually augment over time. Then the flow solution $V(q)$ may gradually transform to periodic or chaotic states with time, and thus the corresponding flow solution $V(q)$ can be treated as an unstable flow state. The stabilities of calculated manifold flow solutions were examined by a time-marching solver as well [28].

3. RESULTS AND DISCUSSION

3.1 Flow Bifurcation in a Curved Tube with Square Cross Section

In this study, 101 × 101 non-isometric grid points were used to analyze a curved tube with a square section in a curvature radius of β = 50; in other words, the section aspect ratio equals 1(γ = 1). In comparison to the results computed by doubled resolution on 202 × 202 grid points, grid independent solutions were practically obtained by 101 × 101 non-equal space grid points. The 101 × 101 grid points are employed for all calculations. Figure 3 is the bifurcation diagram of a curved tube with a square section in terms of the axial velocity at the center point of the section of the curved tube, and the axial pressure gradient less than 6000. As shown in Fig. 3, each branch solution consists of several steady solutions, and several branch solutions form the overall bifurcation diagram. In the figure, limit points and the

https://doi.org/10.1017/jmech.2017.93 Published online by Cambridge University Press

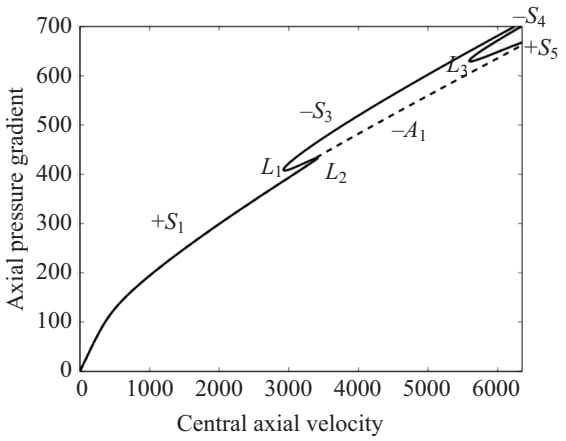


Fig. 3. Divergence curve chart of central axial velocity value and pressure gradient for a square curved tube.

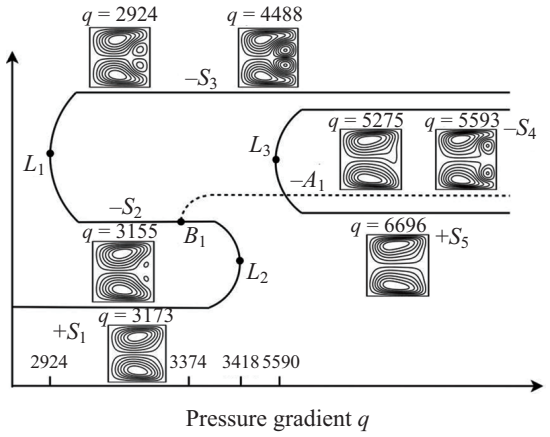


Fig. 4. Reduced divergence curve chart for a square curved tube.

bifurcation point are marked as L and B, respectively, and six individual branch solutions (S_1, S_2, S_3, S_4, S_5 and A_1), three limit points (L_1, L_2 and L_3), and one symmetry-breaking bifurcation point (B_1) can be defined according to the pressure gradient and the flow field pattern inside the curved tube. The flow field pattern in the curved tube can be divided into symmetric and asymmetric flows. The branch solution for the symmetric flow is represented as a solid line, marked as S, while the branch solution for the asymmetric flow is represented as a dotted line, marked as A. Stable branch solutions are marked with +, and unstable branch solutions are marked with −. As shown in the figure, there are limit and bifurcation points when the pressure gradient is between 2900 and 3500, and there is another limit point when the pressure gradient is between 5000 and 6000.

Figure 4 is the schematic bifurcation diagram of Fig. 3 for convenient recognition. It specifically indicates the relative positions and stability states of branch solutions, limit points and bifurcation points in the case of a square curved tube. The cross section flow field patterns corresponding to each branch solution are also included in the figure. With a low pressure gradient, the outer axial velocity of the curved tube is high due to centrifugal action. Therefore, the secondary flow from inside to outside is formed on the symmetric line of the section in order to remedy the pressure drops near the outside. Two symmetrical vortices are formed, which flow anticlockwise and clockwise in the upper and lower parts, respectively, and are symmetrical to the horizontal line at the center of the cavity. The flow field pattern of branch solution S_1 is a stable 2-cell symmetric flow. Via the limit point of L_2 at q = 3418, the 2-cell symmetric flow is destabilized and becomes an unstable S_2 flow state. In the branch solution of S_2, the pressure gradient decreases by degrees from q = 3418, while the flow field pattern still has two large, vertically symmetrical vortices. As the pressure gradient decreases, the range of high outer axial velocity gradually expands. Therefore, in order to remedy the major pressure drop in this region, besides the large vortex formed from the secondary flow from inside to outside of symmetry axis, two small vortices are formed gradually outside the curved tube. They become increasingly apparent, and the range tends to expand, so that the two original large vortices diminish. The flow field pattern of branch solution S_2 is an unstable 4-cell symmetric flow field. In the branch solution, as the pressure gradient increases by degrees from another limit point of L_1 at q = 2924, the two small vortices outside the curved tube gradually expand, and their intensity increases. The flow field pattern of branch solution S_3 is also a symmetric 4-cell flow field.

In addition, for branch solution S_2, when the pressure gradient is q = 3374, there is a branch solution A_1 separated from a symmetry-breaking bifurcation point B_1. In the branch solution for A_1, the pressure gradient gradually increases from q = 3374, and the symmetry breaking caused by the bifurcation point B_1 results in higher axial velocity at the lower outside, so that the upper outside vortex expands towards the lower area. The two small vortices originally observed outside diminish gradually, while the upper large vortices expand and gradually intensify. Finally, the flow field becomes an asymmetric flow field with one large vortex and one small vortex. Therefore, the flow field pattern of the branch solution for A_1 is an unstable 2-cell asymmetric flow field. In addition to the main solution branch, at a high pressure gradient there are two branch solutions, S_4 and S_5, disconnected from the main branch solution. In the branch solution for S_5, the pressure gradient decreases by degrees from q = 6300. The flow field pattern is slightly similar to branch solution S_2, and the flow field has two vortices at its beginning. Two new small vortices are gradually formed in the upper and lower parts outside the curved tube. The two new small vortices intensify and gradually expand as the pressure gradient decreases. The flow field pattern of branch solution S_5 is a stable 2-cell symmetric flow field. When the pressure gradient decreases by degrees to q = 5590, the branch solution of S_4 is entered via limit point L_3, the corresponding flow field pattern is an unstable 4-cell symmetric flow field.

As shown in Fig. 4, when pressure gradient q is present in some regions, the same pressure gradient value has steady solutions for different flow field patterns,

https://doi.org/10.1017/jmech.2017.93 Published online by Cambridge University Press

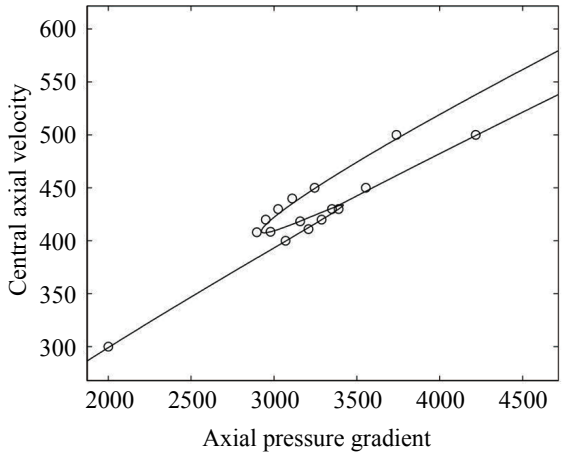


Fig. 5. Flow bifurcation in terms of central axial velocity and pressure gradient in a curved tube with an aspect ratio of 1; o denotes the Winters results [3]. Solid lines denote current computational results.

Table 1. Calculated corresponding pressure gradients of bifurcation points with various aspect ratios for flows within a rectangular curved tube.

Aspect ratio (γ)	The value of pressure gradient			
	L_1	L_2	L_3	B_1
1.40	1108	2103	X	1607
1.35	1196	2338	X	1712
1.30	1296	2678	X	1840
1.25	1413	3170	X	2107
1.20	1559	3883	X	2329
1.19	1593	4061	X	2465
1.18	1632	4251	X	2545
1.17	1667	2095	2634	2092
1.16	1708	2082	2731	2074
1.15	1752	2095	2883	2086
1.13	1848	2159	3059	2146
1.10	2019	2320	3461	2305
1.05	2392	2745	4344	2715
1.00	2924	3418	5590	3374
0.95	3687	4462	7350	4401
0.90	4789	6108	9848	5984

among which only two-cell symmetric flow fields are stable states in branches $+S_1$ and $+S_5$. The 2-cell symmetric flow field can exist in the pressure gradient intervals of 0~3418 and 5590~6000.

Figure 5 compares the flow bifurcation derived from square curved tube with a curvature radius of $\beta = 50$ in this study with the results obtained by Winters [5], who found that the pressure gradient values of corresponding limit points and bifurcation points are $L_1 = 2896$, $B_1 = 3371$, $L_2 = 3416$ and $L_3 = 5564$, respectively. As can be seen in Fig. 5, the results of this study are consistent with those of Winters.

The trends of flow bifurcations might gradually evolve with variance in the aspect ratio. For flow bifurcations of rectangular curved tubes with a curvature radius of $\beta = 50$, the flow field trends in cases with an aspect ratio of 0.9 to 1.17 are similar to that of the case with an aspect ratio of 1. However, when the aspect ratio increases by degrees, the pressure gradient values corresponding to all limit points L_1, L_2 and L_3 and limit point B_1 decrease as the aspect ratio increases. Only the limit point L_2 and bifurcation point B_1 increase with an aspect ratio of between 1.16 and 1.17. The calculated corresponding limit and bifurcation points can be found in Table 1.

3.2 Flow Bifurcation of Curved Rectangular Tube in Aspect Ratio of 1.18 to 1.4

Figure 6 is the divergence curve chart of a rectangular

https://doi.org/10.1017/jmech.2017.93 Published online by Cambridge University Press

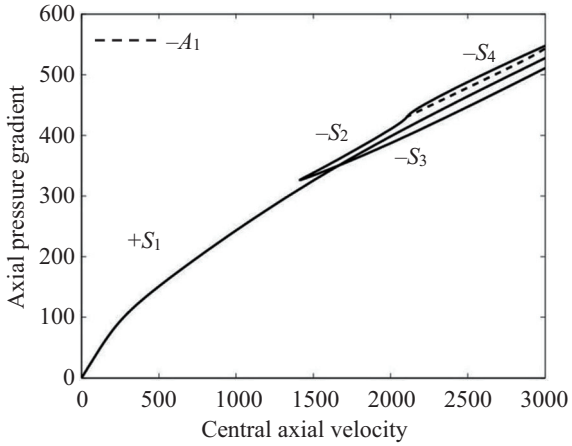


Fig. 6. Flow bifurcation in terms of central axial velocity and pressure gradient in a curved tube with an aspect ratio of 1.25.

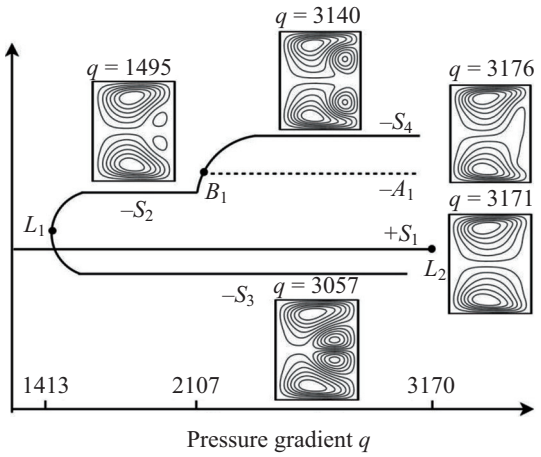


Fig. 7. Reduced divergence curve chart of aspect ratio of 1.25.

curved tube with a curvature radius of $\beta = 50$ and aspect ratio of 1.25, which illustrates the distribution of the central axial velocity of the section of curved tube with a variance in pressure gradient q. A turn occurs when the pressure gradient is 1413, and a bifurcation occurs when the pressure gradient is 2107. Figure 7 is the reduced divergence curve chart of aspect ratio equal to 1.25. When the aspect ratio is in the range from1.18 to 1.4, the reduced divergence curve chart is similar to this type of variation trend. The only difference is the pressure gradient value of limit points and bifurcation points. In this type of divergence curve chart, the flow field in the main branch of $+S_1$ is a stable 2-cell symmetric flow state, disconnected from the other branch solutions. The other branch solutions, $-S_2$, $-S_3$, $-S_4$ and $-A_1$ compose the connected part, and $-S_4$ is connected to $-S_2$ and $-A_1$ by bifurcation point B_1. The flow field patterns of the solution branches of S_2, S_3 and S_4 are part of an unstable 4-cell symmetric flow state. The flow pattern of the branch solution A_1 is an asymmetric flow state. In this case, as the outside axial velocity in the upper area is higher, the lower vortices expand upwards, thus resulting in an asymmetric flow field with lower vortices larger than upper vortices. Therefore, the flow field pattern of A_1 is an unstable 2-cell asymmetric flow field. It should be noted that, in this study, the unstable solutions gotten by the continuation method only reveal the relationships and evolutions between every stable solution in the bifurcation diagrams. Because the unsteady terms were not considered in the governing equations, steady state solutions including stable and unstable solutions can be obtained by the solver. By the stability analysis, the stability of the steady state solutions can be further distinguished. In the experiments, only stable solutions can be observed, and the unstable stable solutions cannot appear stably because their instable characteristics in terms of time aspect. By instituting the calculated unstable solutions as an initial estimate into a time-marching solver, the solver may attain to the other convergent stable solutions or time-depending solutions depending on the corresponding pressure gradient parameters [27]. In this study, only stable solutions and their existence

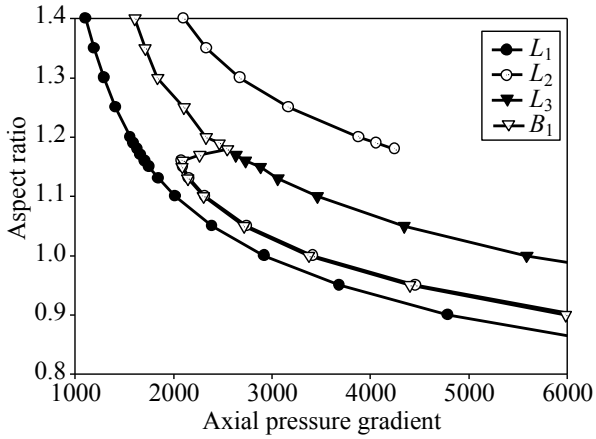


Fig. 8. Relation of pressure gradients of limit points and bifurcation point to aspect ratio.

region in terms of aspect ratio and pressure gradient are our major concerns.

Figure 8 shows the variation of limit points L_1, L_2 and L_3 and bifurcation point B_1 with the pressure gradient and aspect ratio in the flow bifurcation of a rectangular curved tube with a curvature radius of $\beta = 50$ and aspect ratio of 0.9 to 1.4. In terms of limit point L_1, the pressure gradient value corresponding to L_1 decreases as the aspect ratio increases. As the aspect ratio increases from 0.9 to 1.4, the pressure gradient value corresponding to L_1 decreases from 4789 to 1108. In terms of limit point L_2, the pressure gradient value corresponding to L_2 also decreases as the aspect ratio increases. However, when the aspect ratio is 1.18, a sudden jump on the pressure gradient of L_2 appears. In terms of bifurcation point, when the aspect ratio is less than 1.17, the pressure gradient value corresponding to B_1 gradually decreases as the aspect ratio increases. However, when the aspect ratio is between 1.17 and 1.18, the distributions of pressure gradient value of B_1 show a sudden jump from q = 2090 to q = 2545. When the aspect ratio is greater than 1.17, the pressure gradient value of B_1 also decreases as

https://doi.org/10.1017/jmech.2017.93 Published online by Cambridge University Press

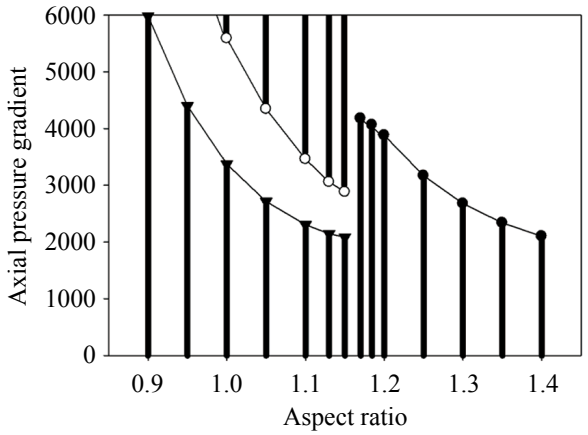


Fig. 9. Regions of steady flow field in pressure gradient inside rectangular curved tube with aspect ratio of 0.90 to 1.40.

the aspect ratio increases. As shown in Fig. 7, when the aspect ratio is lower than 1.18, the distributions of bifurcation point B_1 and limit point L_3 form a thumb-shaped curve.

Figure 9 shows the regions of steady-state flow field in pressure gradient when the aspect ratio is 0.90 to 1.40. As shown, when the aspect ratio is in the range of 0.9 to 1.18, the regions of steady-state flow field are in two distinct sections, and the flow states in the blank area in the figure are unstable flows. When the aspect ratio is in the range of 1.18 to 1.4, there is a steady flow field in only one section at a lower pressure gradient. When the aspect ratio is in the range of 0.90 to 1.18, the corresponding flow field patterns are stable 2-cell symmetric flow fields, as the flow bifurcation has branch solutions S_1 and S_5 of two steady flow fields, as shown in Fig. 4. The existence interval of S_1 decreases as the aspect ratio increases in this range of aspect ratio. The minimum pressure gradient value corresponding to the existence range of the S_5 branch solution decreases as the aspect ratio increases as well, so the existence interval of S_5 gradually expands towards low pressure gradient range as the aspect ratio increases, as shown in Fig. 9. When the aspect ratio is 1.18 to 1.40, there is only one branch solution S_1 that is a stable steady flow field, as shown in Fig. 7, and the corresponding flow field pattern is a 2-cell symmetric flow field. The existence interval of S_1 decreases as the aspect ratio increases in this range of aspect ratio. The existence interval of S_1 mostly decreases as the aspect ratio increases. However, in cases where the aspect ratio is 1.17 or 1.18, there is a large variance in pressure gradient intervals where the stable 2-cell symmetric flow states exist, which are 0~2095 and 0~4251. Thus, it is between these aspect ratios that the divergence curve chart obviously changes. As shown in Fig. 9, in the middle blank section of the first aspect ratio range and in the upper blank section of the second aspect ratio range, no other stable flow field solutions are found. In these regions, three dimensional or time dependent effects may occur, and prevent the acquisition of steady solutions by the current numerical solver.

4. CONCLUSIONS

This study discussed the changes in laminar flow within a curved tube with a rectangular section, with a fixed curvature radius (β = 50) and different section aspect ratios. The difference method was used for discretization, and pressure gradient ($1 \leqslant q \leqslant 6000$) was used as the continuation parameter to trace the solution curves. First, the flow fields in the curved tube with a square section were discussed, and three limit points and one symmetry-breaking point were identified, while the ranges in the pressure gradient of the stable 2-cell symmetric flow field were distinguished.

The evolution of bifurcation diagrams in terms of aspect ratio and pressure gradient was also illustrated. According to the similarity of the bifurcation diagrams in terms of aspect ratio, the bifurcation diagrams were classified into two types. Furthermore, from the evolution of bifurcation diagrams, the existing regions of the stable flow state were determined in terms of pressure gradient and aspect ratio.

In cases with an aspect ratio of 1.17 or 1.18, there was a large variation in bifurcation diagram and pressure gradient intervals where there were stable 2-cell symmetric flow states. When the aspect ratio was in the range of 0.9 to 1.18, the regions of the stable flow field appeared as two distinct sections between which an unstable 4-cell and asymmetric flow field was observed. When the aspect ratio was in the range of 1.18 to 1.4, the steady flow field was observed only in one section at a lower pressure gradient, beyond which time-dependent flow state may occur in addition to the unstable 4-cell and asymmetric flow fields. The calculation results are beneficial to engineers, assisting in understanding flow fields in curved rectangular tubes in terms of pressure gradient and aspect ratio, and in improved design of suitable geometric and operational parameters for tube flow in various applications.

ACKNOWLEDGEMENTS

The author gratefully acknowledges the financial support provided by the National Science Council of Taiwan under Grant Nos. NSC 102-2221-E-167-021-MY2 and NSC 103-2622-E-167-002-CC2 for this study.

REFERENCES

1. Dean, W. R., "The Stream-Line Motion of Fluid in a Curved Pipe," *The London, Edinburgh, and Dublin Philosophical Magazine and Journal of Science: Series 7*, **5**, pp. 673-695 (1928).
2. Joseph, B., Smith, E. P. and Adler, R. J., "Numerical Treatment of Laminar Flow in Helically Coiled Tubes of Square Cross-Section," *AIChE Journal*, **21**, pp. 965-974 (1975).
3. Cheng, K. C., Lin, R. C. and Ou, J. W., "Fully-

https://doi.org/10.1017/jmech.2017.93 Published online by Cambridge University Press

Developed Laminar Flow in Curved Rectangular Channels," *Journal of Fluids Engineering*, **98**, pp. 41-48 (1976).

4. Hille, P., Vehrenkamp, R. and Schulz-Dubois, E. O., "The Development and Structure of Primary and Secondary Flow in a Curved Square Duct," *Journal of Fluid Mechanics*, **151**, pp. 219-241 (1985).
5. Winters, K. H., "A Bifurcation Study of Laminar Flow in a Curved Tube of Rectangular Cross- Section," *Journal of Fluid Mechanics*, **180**, pp. 343-369 (1987).
6. Gauthier, G., Gondret, P., Thomé, H. and Rabaud, M., "Centrifugal Instabilities in a Curved Rectangular Duct of Small Aspect ratio," *Physics of Fluids*, **13**, pp. 2831-2834 (2001).
7. Yanase, S., Kaga, Y. and Daikai, R., "Laminar Flow through a Curved Rectangular Duct over a Wide Range of the Aspect Ratio," *Fluid Dynamics Research*, **31**, pp. 151-183 (2002).
8. Yamamoto, K., Wu, X., Hyakutake, T. and Yanase, S., "Taylor-Dean Flow through a Curved Duct of Square Cross Section," *Fluid Dynamics Research*, **35**, pp. 676-82 (2004).
9. Yamamoto, K., Wu, X., Nozaki, K. and Hayamizu Y., "Visualization of Taylor-Dean Flow in a Curved Duct of Square Cross-Section," *Fluid Dynamics Research*, **38**, pp. 1-18 (2006).
10. Bhunla, A. and Chen, C. L., "Flow Characteristics in a Curved Rectangular Channel with Variable Cross-Sectional Area," *Journal of Fluid Engineering*, **131**, 091102 (2009).
11. Norouzi, M., Kayhani, M. H., Shu, C. and Nobari, M .R. H., "Flow of Second-Order Fluid in a Curved Duct with Square Cross-Section," *Journal of Non-Newtonian Fluid Mechanics*, **165**, pp. 323-339 (2010).
12. Norouzi, M. and Biglari, N., "An Analytical Solution for Dean Flow in Curved Ducts with Rectangular Cross Section," *Physics of Fluids*, **25**, 053602 (2013).
13. Wang, L. and Yang, T., "Periodic Oscillation in Curved Duct Flows," *Physica D*, **200**, pp. 296-302 (2005).
14. Mondal, R. N., Kaga, Y., Hyakutake, T. and Yanase, S., "Bifurcation Diagram for Two-Dimensional Steady Flow and Unsteady Solutions in a Curved Square Duct," *Fluid Dynamics Research*, **39**, pp. 413-446 (2007).
15. Komai, Y. and Tanishita, K., "Fully Developed Intermittent Flow in a Curved Tube," *Journal of Fluid Mechanics*, **347**, pp. 263-287 (1997).
16. Hüttl, T. J. and Friedrich, R., "Influence of Curvature and Torsion on Turbulent Flow in Helically Coiled Pipes," *International Journal of Heat and Fluid Flow*, **21**, pp. 345-353 (2000).
17. Cioncolini, A. and Santini, L., "On the Laminar to Turbulent Flow Transition in Diabatic Helically Coiled Pipe Flow," *Experimental Thermal and Fluid Science*, **30**, pp. 653-661 (2006).
18. Ko, T. H. and Ting, K., "Optimal Reynolds Number for the Fully Developed Laminar Forced Convection in a Helical Coiled Tube," *Energy*, **31**, pp. 2142-2152 (2006).
19. Liu, F. and Wang, L., "Analysis on Multiplicity and Stability of Convective Heat Transfer in Tightly Curved Rectangular Ducts," *International Journal of Heat and Mass Transfer*, **52**, pp. 5849-5866 (2009).
20. Mondal, R. N., Uddin, M. S. and Yanase, S., "Numerical Prediction of Non-Isothermal Flow through a Curved Square Duct," *International Journal of Fluid Mechanics Research*, **37**, pp. 85-99 (2010).
21. Mondal, R. N., Islam, S., Uddin, K. and Hossain, A., "Effects of Aspect Ratio on Unsteady Solutions through Curved Duct Flow," *Applied Mathematics and Mechanics*, **34**, pp. 1107-1122 (2013).
22. Keller, H. B., *Numerical Solution of Bifurcation and Nonlinear Eigenvalue Problems, In Applications of Bifurcation Theory,* Rabinowitz, P. Ed., pp. 359-384, Academic Press, New York (1977).
23. Yang, R.-J. and Luo, W.-J., "Flow Bifurcations in a Thin Gap between Two Rotating Spheres," *Theoretical and Computational Fluid Dynamics*, **16**, pp. 115-131 (2002).
24. Luo, W.-J. and Yang, R.-J., "Multiple Fluid Flow and Heat Transfer Solutions in a Two-Sided Lid-Driven Cavity," *International Journal of Heat and Mass Transfer*, **50**, pp. 2394-2405 (2007).
25. Chen, K. T., Tsai, C. C., Luo, W. J. and Chen, C. N., "Multiplicity of Steady Solutions in a Two-Sided Lid-Driven Cavity with Different Aspect Ratios," *Theoretical and Computational Fluid Dynamics*, **27**, pp. 767-776 (2013).
26. Chen, K. T., Tsai, C. C., Luo, W. J., Lu, C. W. and Chen, C. H., "Aspect Ratio Effect on Multiple Flow Solutions in a Two-Sided Parallel Motion Lid-Driven Cavity," *Journal of Mechanics*, **31**, pp.1-8 (2015).
27. Sorensen, D. C., "Implicit Application of Polynomial Filters in a k-Step Arnoldi Method," *SIAM Journal on Matrix Analysis and Applications*, **13**, pp. 357-367 (1992).
28. Luo, W. J., "Transient Electroosmotic Flow Induced by dc or ac Electric Fields in a Curved Micro-Tube," *Journal of Colloid and Interface Science*, **278**, pp. 497-507 (2004).

(Manuscript received February 19, 2016,
accepted for publication September 12, 2017.)

https://doi.org/10.1017/jmech.2017.93 Published online by Cambridge University Press